Biochimica et Biophysica Acta 1807 (2011) 59–67

Contents lists available at ScienceDirect

Biochimica et Biophysica Acta

journal homepage: www.elsevier.com/locate/bbabio

The transmembrane domain 6 of vacuolar H^+-pyrophosphatase mediates protein targeting and proton transport

Yih-Jiuan Pan, Chien-Hsien Lee, Shen-Hsing Hsu, Yun-Tzu Huang, Ching-Hung Lee, Tseng-Huang Liu, Yen-Wei Chen, Shih-Ming Lin, Rong-Long Pan *

Department of Life Science and Institute of Bioinformatics and Structural Biology, College of Life Science, National Tsing Hua University, Hsin Chu 30043, Taiwan, Republic of China

ARTICLE INFO

Article history:
Received 12 June 2010
Received in revised form 1 October 2010
Accepted 5 October 2010
Available online 16 October 2010

Keywords:
Proton translocation
Tonoplast
Vacuole
Vacuolar H^+-pyrophosphatase
Site-directed mutagenesis

ABSTRACT

Vacuolar H^+-pyrophosphatase (V-PPase; EC 3.6.1.1) plays a significant role in the maintenance of the pH in cytoplasm and vacuoles via proton translocation from the cytosol to the vacuolar lumen at the expense of PP_i hydrolysis. The topology of V-PPase as predicted by TopPred II suggests that the catalytic site is putatively located in loop e and exposed to the cytosol. The adjacent transmembrane domain 6 (TM6) is highly conserved and believed to participate in the catalytic function and conformational stability of V-PPase. In this study, alanine-scanning mutagenesis along TM6 of the mung bean V-PPase was carried out to identify its structural and functional role. Mutants Y299A, A306S and L317A exhibited gross impairment in both PP_i hydrolysis and proton translocation. Meanwhile, mutations at L307 and N318 completely abolished the targeting of the enzyme, causing broad cytosolic localization and implicating a possible role of these residues in protein translocation. The location of these amino acid residues was on the same side of the helix wheel, suggesting their involvement in maintaining the stability of enzyme conformation. G297A, E301A and A305S mutants showed declines in proton translocation but not in PP_i hydrolysis, consequently resulting in decreases in the coupling efficiency. These amino acid residues cluster at one face of the helix wheel, indicating their direct/indirect participation in proton translocation. Taken together, these data indicate that TM6 is crucial to vacuolar H^+-pyrophosphatase, probably mediating protein targeting, proton transport, and the maintenance of enzyme structure.

1. Introduction

Vacuolar H^+-pyrophosphatase (V-PPase; EC 3.6.1.1) catalyzes electrogenic H^+-translocation from the cytosol to the vacuolar lumen at the expense of hydrolysis of inorganic pyrophosphate (PP_i). V-PPase is found mainly in higher plants, some protozoa, and several species of archae, eubacteria, eukarya and prokarya [1–3]. The cDNA and amino acid sequences of V-PPase from different species possess a high degree of homology and identity [3]. V-PPase contains two identical subunits whose molecular mass is approximately 75–81 kDa [3–5]. Hydropathic and membrane topological analyses indicate that V-PPase consists of 14–17 transmembrane domains, and its putative catalytic loops presumably face the cytosolic side [2,6]. It has been shown that the physiological substrate for V-PPase is a Mg^{2+}-PP_i complex (Mg_2PP_i); indeed, binding of Mg^{2+} activates and stabilizes the V-PPase [3,7]. The enzymatic activity of V-PPase can be stimulated by high concentrations of K^+ but inhibited by Ca^{2+}, Na^+, and F^- [3]. V-PPase likely contains domains for binding substrate and the above ligands, as well as domains for proton translocation. Recently, a novel and K^+-independent subclass of V-PPases from *Arabidopsis*, *R. rubrum*, and *P. aerophilum* was discovered [2,8–10]. However, the essential regions of V-PPases for enzymatic function, proton translocation and ion binding have not yet been determined.

Many important residues involved in the enzymatic and proton translocating reactions of V-PPase have been identified using sitety-directed mutagenesis. For instance, the three charged residues Asp253, Lys261, and Glu263 are crucial for enzymatic activity [3]. Using mutation and biochemical assays, it was also revealed that Glu305 and Asp504 of *Arabidopsis thaliana* V-PPase directly participate in DCCD binding and are presumably critical for catalysis [11]. Moreover, a fragment of DX_7KXE on loop e of V-PPase has been implicated as the universal PP_i-binding motif [12]. Two consensus acidic regions, expressed as a common motif DX_3DX_3D on both loops e and m of the cytosolic side, may play roles in the binding of the substrate complex Mg_2PP_i [12]. It was further shown that K261 and E263 might be involved in the energy conversion from enzymatic reaction to proton transport, and that the second acidic region (on loop m) is also involved in PP_i hydrolysis [12].

The topology of mung bean V-PPase was predicted by TopPred II with minor modifications, as shown in Fig. 1A [cf., 13]. The catalytic site for substrate hydrolysis is presumably located in loop e, between transmembrane domains 5 (TM5) and 6 (TM6), and is exposed to the cytosol. TM5 contains a GYG motif that plays a role in maintaining the

Abbreviations: DCCD, *N,N'*-dicyclohexylcarbodiimide; DTT, dithio-threitol; EGTA, ethyleneglycol-bis-(β-amino-ethylether) *N,N,N',N'*-tetraacetic acid; PMSF, phenyl-methylsulfonyl fluoride; V-PPase, vacuolar H^+-pyrophosphatase

* Corresponding author. Tel./fax: +886 3 5742688.
E-mail address: rlpan@life.nthu.edu.tw (R.-L. Pan).

0005-2728/$ – see front matter © 2010 Elsevier B.V. All rights reserved.
doi:10.1016/j.bbabio.2010.10.006

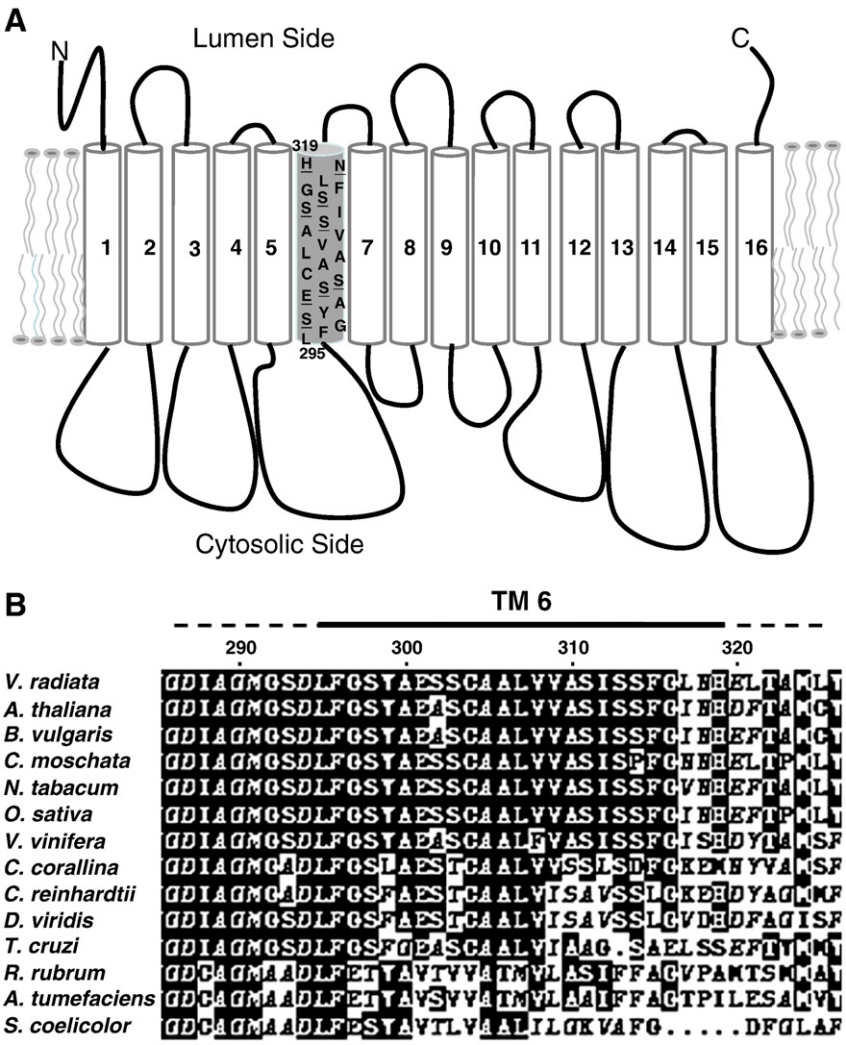

Fig. 1. The predicted topology of V-PPase and multiple sequence alignment of various organisms. (A) The topology of V-PPase. (B) The sequence alignments. The topology of V-PPase predicted by TopPred II indicates the sequence of transmembrane domain 6 with underlines for hydrophilic residues. Amino acid sequences of V-PPases from various organisms are aligned using "the Biology Workbench 3.2" [32]. The GenBank accession numbers for V-PPases of each species are: *Vigna radiata*, P21616; *Arabidopsis thaliana*, BAA32210; *Beta vulgaris*, AAA61609; *Cucurbita moschata*, BAA33149; *Nicotiana tabacum*, CAA58700; *Oryza sativa*, BAA31523; *Vitis vinifera*, AAF69010; *Chara coralline*, BBA36841; *Chlamydomonas reinhardtii*, CAC44451; *Dunaliella viridis*, ADK36629; *Trypanosoma cruzi*, XP_814868; *Rhodospirillum rubrum*, AAC38615; *Agrobacterium tumefaciens*, AAK86977; *Streptomyces coelicolor*, Q9X913.

structure and function of V-PPase [14]. Furthermore, TM6 is highly conserved in higher plants, as revealed by multiple sequence alignment (Fig. 1B), but it is relatively low in hydrophobicity as compared to other transmembrane fragments. It is believed that TM6 is probably involved in enzymatic function, proton translocation and/or the stability of enzyme structure. To verify these possibilities, this study aimed to determine the role of TM6 in mung bean V-PPase by alanine scanning. Different amino acids of TM6 were individually substituted by alanine, and alanine residues were substituted by serine. A series of site-directed mutants were constructed, over-expressed in *Saccharomyces cerevisiae*, and then used to determine their enzymatic activities and proton translocations. The role of each amino acid along TM6 was examined and a working model for this fragment is proposed.

2. Materials and methods

2.1. Microorganisms and plasmids

Escherichia coli strain XL1-Blue (*rec*A1, *end*A1, *gyr*A96, *thi*-1, *hsd*R17 (r_k^-, m_k^+), *sup*E44, *rel*A1, lac [F' *pro*AB, $lac^qZ\Delta M15$, Tn10 (tet^r)]) was employed for the amplification of plasmids. XL1-Blue harboring plasmids were grown in Luria broth (LB, [0.5% (w/v) yeast extract, 1% (w/v) tryptone and 1% (w/v) NaCl]) or on LB plates containing 50 μg ml^{-1} ampicillin. A vacuolar protease-deficient haploid *S. cerevisiae* strain BJ2168 (*MATa, prc1-407, prb1-1122, pep4-3, leu2, trp1, ura3-52*) was used for the heterologous expression of the mung bean (*Vigna radiata* L.) V-PPase (Accession number P21616) [15]. BJ2168 was grown in CM medium [0.2% (w/v) yeast nitrogen base without amino acids and ammonium sulfate, 0.5% (w/v) ammonium sulfate, 2% (w/v) glucose or galactose, 0.01% (w/v) leucine and 0.01% (w/v) tryptophan]. Plasmids pBV was constructed by cloning V-PPase gene into pBlueScript II SK (+) between *Hind*III and *Xba*I sites for generating mutants in following studies. The mutated V-PPase cDNA was then subcloned into an *E. coli*/*S. cerevisiae* shuttle vector, pYES2 (Invitrogen, Carlsbad, CA, USA) after *GAL1* promoter between *Hind*III and *Xba*I. Tag containing 6 His was then subcloned into plasmids before heterologous expression in *S. cerevisiae*.

2.2. Mutagenesis and DNA manipulation

Mutants were generated by the PCR MegaPrimer method [16] and QuickChange PCR mutagenesis (Stratagene, La Jolla, CA, USA).

Mutagenic and antisense standard primers used in this study were shown and the presence of mutated residues underlined as follows:

L295A 5'-GGGATCTGATGCGTTTGGTTCATATGC-3'
L295A-R 5'-GCATATGAACCAAACGCATCAGATCCC-3'
F296A 5'-GGATCTGATCTGGCTGGTTCATATGCG-3'
F296A-R 5'-CGCATATGAACCAGCCAGATCAGATCC-3'
G297A 5'-CTGATCTGTTTGCTTCATATGCGGAGTC-3'
G297A-R 5'-GACTCCGCATATGAAGCAAACAGATCAG-3'
S298A 5'-GATCTGTTTGGTGCTTATGCGGAGTCATC-3'
S298A-R 5'-GATGACTCCGCATAAGCACCAAACAGATC-3'
Y299A, 5'-GTTTGGTTCAGCAGCGGAGTC-3'
A300S, 5'-GGTTCATATTCGGAGTCATCTTG-3'
E301A, 5'-CATATGCGGCGTCATCTTGTG-3'
S302A, 5'-CATATGCGGAGGCTTCTTGTGC-3'
S303A, 5'-CATATGCGGAGTCTGCTTGTGC-3'
C304A, 5'-GGAGTCATCTGCTGCTGCTCTTG-3'
A305S, 5'-GAGTCATCTTGTTCTGCTCTTGTTG-3'
A306S, 5'-CATCTTGTGCTTCTCTTGTTGTTGC-3'
L307A, 5'-CTTGTGCTGCTGCTGTTGTTGC-3'
V308A, 5'-GTGCTGCTCTTGCTGTTGCTTC-3'
V309A, 5'-GCTCTTGTTGCTGCTTCCATC-3'
A310S, 5'-CTCTTGTTGTCTCCTCCATCTCTTC-3'
S311A, 5'-CTTGTTGTTGCTGCCATCTCTTC-3'
I312A, 5'-GTTGCTTCCGCCTCTTCATTTG-3'
S313A, 5'-GTTGCTTCCATCGCTTCATTTG-3'
S314A, 5'-CCATCTCTGCCTTTGGGTTG-3'
F315A, 5'-CATCTCTTCTGCTGGCTTGAATCAC-3'
G316A, 5'-CTTCATTTGCCTTGAATCACGAG-3'
L317A, 5'-CTTCATTTGGAGCGAATCACGAG-3'
N318A, 5'-CATTTGGGTTAGCACACGAGTTG-3'
H319A, 5'-GTTGAATGCCGAGTTGACTGC-3'
PstuI544 5'-GGGAAGGCCTTCATTACGGC-3'
Re1239 5'-CCCAAAGACCAACAGCAACAC-3'

All the polymerase chain reactions were carried out using the PCR machine Mastercycler (Eppendorf AG, Westbury, New York, USA). The final Megaprimer PCR products were cut with *Aat*II and *Stu*I, and cloned back to pBV. The QuickChange PCR products were treated with *Dpn*I to digest the parental (non-mutated) DNA. Following the confirmation of sequence, the V-PPase cDNAs were inserted into pYES2 vector for transformation of the yeast.

2.3. Preparation of microsomes, enzyme assay, and protein determination

Crude membrane fractions were prepared from the heterologously expressing yeast cells with minor modifications as described previously [cf., 17,18]. The yeast microsomes were finally resuspended in the storage buffer and stored at −80 °C for further use. PP_i hydrolytic activity was measured as the liberation of P_i from PP_i as described previously [18]. Lineweaver–Burk plot was obtained conventionally and values of K_M and V_{max} were thus determined using Sigmaplot 7.0 software (SPSS, Chicago, IL, USA). Protein content was determined by a modified Bradford method with BSA as the standard [19].

2.4. Measurement of PP_i-dependent H^+ translocation

Proton translocation was measured as fluorescence quenching of acridine orange (the excitation wavelength 490 nm, the emission wavelength 530 nm) using Hitachi F-4000 fluorescence spectrophotometer (Hitachi Ltd., Tokyo, Japan). Reaction mixture for proton translocation contained 5 mM Tris–HCl (pH 8.0), 1 mM EGTA-Tris (pH 7.6), 400 mM glycerol, 100 mM KCl, 1.3 mM $MgSO_4$, 5 μM acridine orange, and 50 μg ml^{-1} microsomal proteins. The fluorescence quenching was initiated by adding 1 mM sodium pyrophosphate (pH 7.6). The ionophore, gramicidin D (5 μg ml^{-1}), was included at end of each assay to stop the reaction and to confirm the integrity of the membrane. The coupling ratio (the ratio of proton pumping to the rate of PP_i hydrolysis) was then measured as ($\triangle F\ \%\ min^{-1}$) (μmol PP_i hydrolyzed min^{-1})$^{-1}$[11].

2.5. SDS-PAGE and Western blotting analysis

SDS-PAGE was performed according to Laemmli with minor modifications [20,21]. The proteins on gels were visualized with silver stain or electrotransferred to polyvinylidene difluoride membrane (PVDF) using the semi-dry electrotransblotting apparatus (Nova Blot, Amersham Pharmacia Biotech, Piscataway, NJ, USA). The PVDF membrane was then incubated with anti-His antibody for 2 h. Following three washes, the membrane was treated with the goat anti-mouse IgG-conjugated horseradish peroxidase. Bands of immunoblot were visualized using the Western Lightning™ kit (New England Nuclear, Boston, MA, USA) as recommended by the manufacturer.

2.6. Immunofluorescence

S. cerevisiae immunostaining was performed according to the method previously described [22] with minor modifications. In brief, the yeast cells were grown under conditions as mentioned above. Samples were cross-linked by formaldehyde (5% (v/v)), washed twice with PBS and made spheroplasts with lyticase [100 μg ml^{-1} lyticase (Sigma L4025), 3 μg ml^{-1} PMSF, 2 μl ml^{-1} β-mercaptoethanol]. Cells were applied onto polylysine-coated slides and fixed at −20 °C by methanol for 5 min. Cells were then permeabilized in a PBS-based wash buffer containing 0.1% (v/v) Triton X-100. For immunofluorescence, primary and secondary antibody layers were applied in blocking buffer [2% (w/v) BSA and 0.1% (v/v) Tween 20 in PBS]. The primary antibody is mouse anti-His antibody [(GenScript A00186; Piscataway, NJ, USA); 1:100 dilution; overnight], and the secondary antibody is Alexa Fluor 633 goat anti-mouse IgG [(Invitrogen A21052; Carlsbad, CA, USA); 1:500 dilution; 1–2 h]. Confocal images were taken with Zeiss LSM 510 confocal microscope (Carl Zeiss, Inc., Jena, Germany).

2.7. Trypsin proteolysis

The TPCK-treated trypsin (Promega, Madison, WI, USA) was dissolved in 50 mM acetic acid to make 100 μg ml^{-1} of stock solution. The microsomal proteins (30 μg) were incubated with fresh trypsin solution at ratio of 50:1 (w/w) at 37 °C for 15 min. The proteolysis was stopped by adding the denaturation buffer containing 10% (w/v) SDS, 5% (w/v) β-mercaptoethanol, 50 mM Tris–HCl (pH 6.8), 10% (w/v) glycerol, 0.002% (w/v) bromophenol blue and 5 mM PMSF, followed by heating at 65 °C for 10 min. The samples were subjected immediately to 12.5% (w/v) SDS-PAGE and Western blotting analysis performed as described above.

2.8. Control over K^+, Na^+, and Ca^{2+} contamination

The background concentrations of K^+, Na^+, and Ca^{2+} in our assay media were below 4.0, 5.0 and 20 nM, respectively, as determined by inductively coupled plasma-atomic emission spectrometer (ICP-AES) at NTHU Instrument Center, National Tsing Hua University, Hsin Chu, Taiwan.

3. Results

3.1. Expression and function of TM6 mutants

The cDNA encoding mung bean vacuolar H^+-PPase (VVP) was inserted into the yeast expression shuttle vector pYES2 and transcribed efficiently in yeast under the control of *GAL1* regulatory promoter [cf., 11,17,21,23]. The partially purified membrane preparations displayed PP_i hydrolysis and associated proton translocation, in agreement with results from previous studies [14,18,24]. Residues along TM6 of the mung bean vacuolar H^+-PPase (from L295 to H319) were individually replaced by alanine, and the original alanine residues on the fragment were substituted by serine. The expressed V-PPase variants, except for Y299A, A306S, L307A, L317A and N318A mutants, were visualized as a 73-kDa protein by Western blotting (Fig. 2A). The efficiency of expression in yeast was similar regardless of the mutation. The mutants that did not express grew normally on selection plate (Fig. 3A), implicating the presence of the selection marker in the vectors. The plasmids of these mutants were rescued and re-transformed into *E. coli*, demonstrating that they still contained the VVP gene (data not shown). The absence of these proteins in Western blotting might be explained by the loss of V-PPase before targeting the membranes.

Furthermore, PP_i hydrolysis and the associated proton translocation of microsomes from all mutants were measured, as shown in Fig. 2B and C, respectively. The microsomal membranes of the wild-type strain showed high PP_i hydrolysis and PP_i-dependent H^+ transport activities of 41.3 ± 0.5 μmol PP_i (mg protein · h)$^{-1}$ and

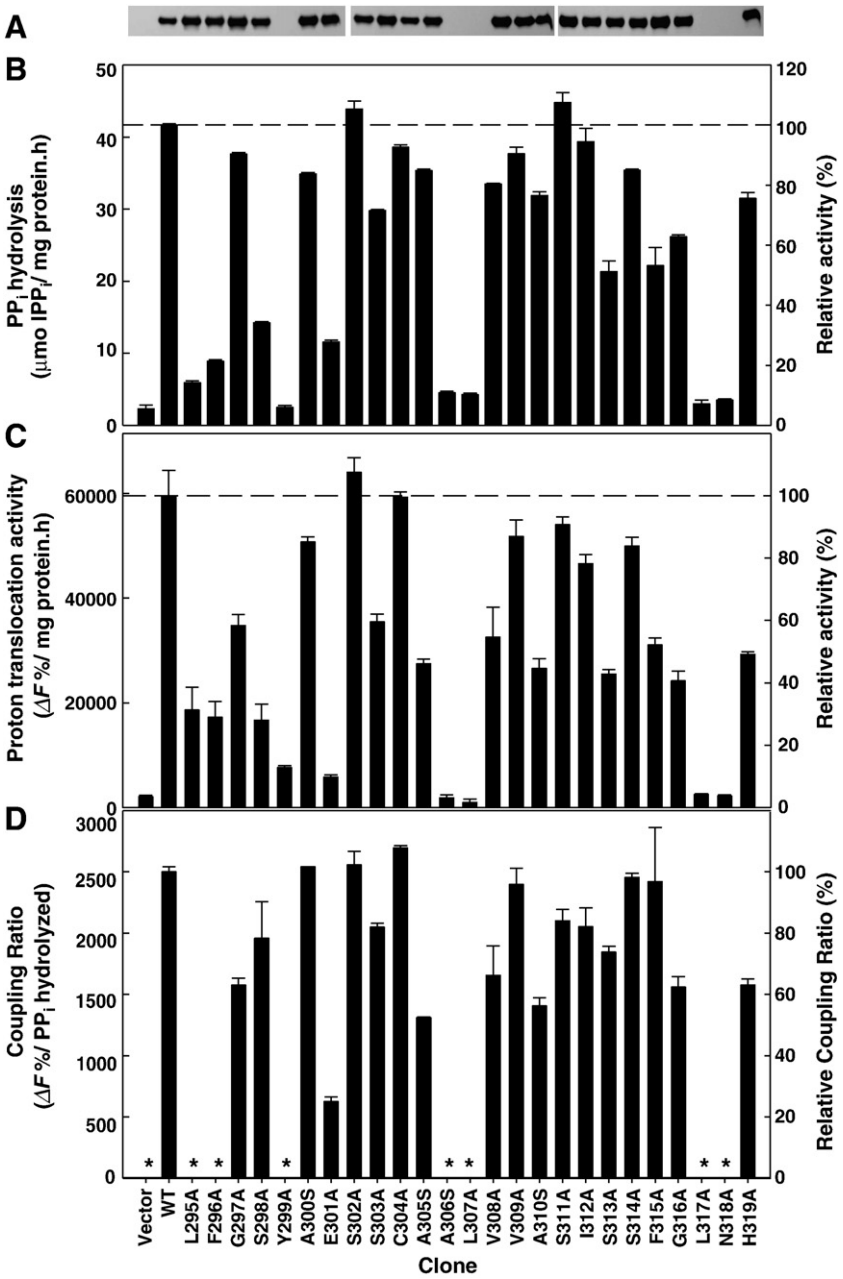

Fig. 2. Heterologous expression of mutant V-PPases and their enzymatic activities. (A) The expression level shown by Western blot. (B) PP_i hydrolysis activity. (C) PP_i-dependent proton translocation. (D) Relative coupling ratios. Membrane fractions were prepared from *S. cerevisiae* BJ2168 expressing wild-type and mutated V-PPases as indicated. Thirty microgram microsomal fractions of each mutant were visualized by Western blotting with anti-His antibody. Coupling ratio is expressed as ($\triangle F\%$ min^{-1}) (μmol PP_i hydrolyzed min^{-1})$^{-1}$, where $\triangle F\%$ min^{-1} is the initial rate of relative fluorescence quenching of acridine orange. The asterisk symbols (*) indicate not determined. Data are shown as means ± standard deviation from at least three separate experiments.

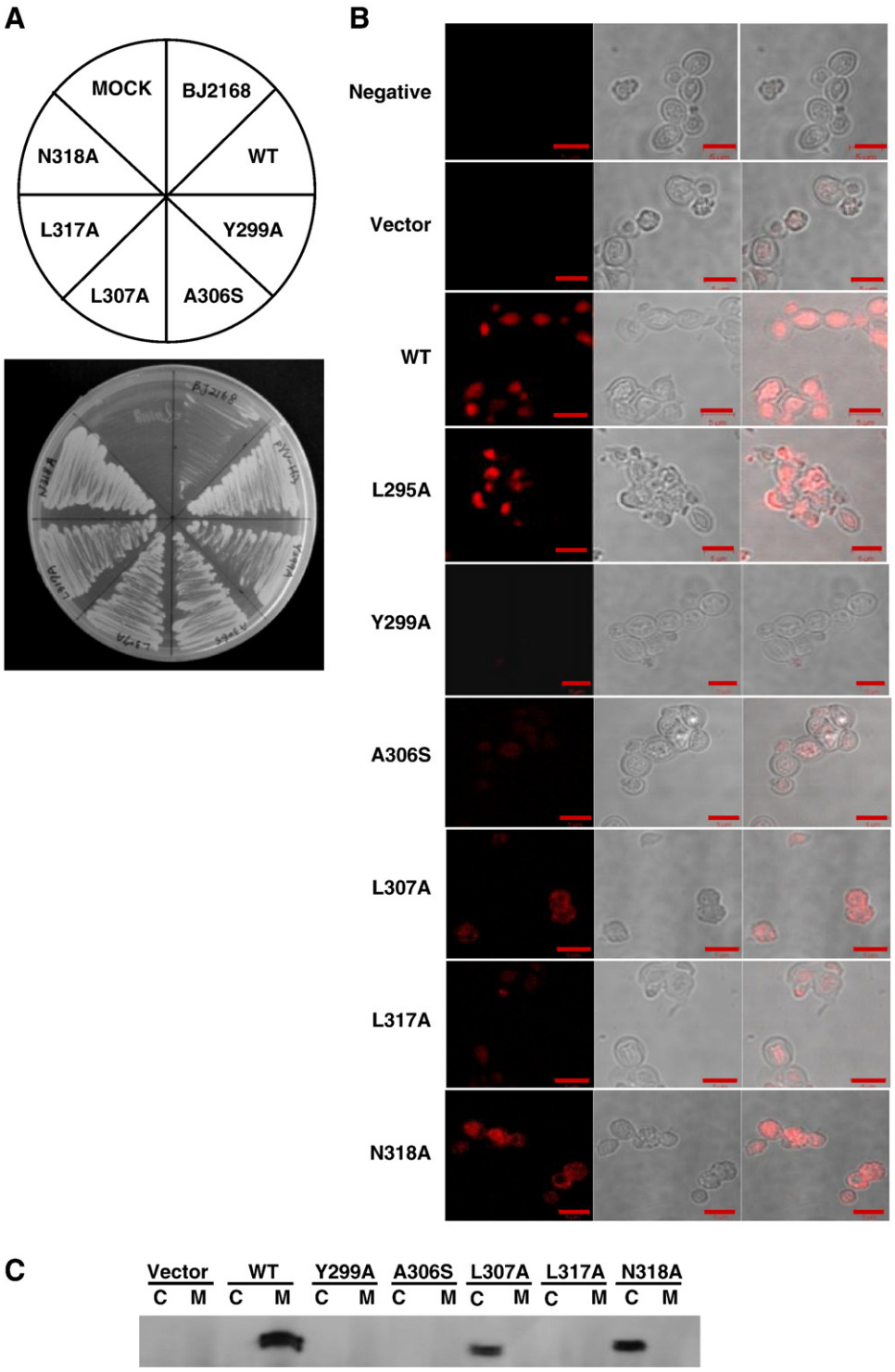

Fig. 3. The plate growth and subcellular localization of mutant V-PPases. (A) The growth of mutated V-PPases in selected agar plate. (B) Immunolocalization by indirect immunofluorescence. (C) Recognition of mutant V-PPases in soluble or membrane fractions. The spheroblasts were immunostained with primary [mouse anti-His antibody (1:100 dilution; overnight)] and secondary [Alexa Fluor 633 goat anti-mouse IgG (1:500 dilution; 1–2 h)] antibodies consecutively, as described under Materials and methods. The negative control, wild-type yeast cell stained with secondary antibody alone, was used to ensure that no non-specific binding to V-PPase occurred. The images are in pairs with fluorescence on the left column, bright field on the middle column, and merges on the right column. Scale bars, 5 μm. Equivalent amounts of cytosolic (C) and membrane (M) fractions were loaded in each lane. The expression of mutant V-PPases was visualized by Western blotting with anti-His antibody.

$59.5\times10^3\pm4.8\times10^3$ ΔF% (mg protein · h)$^{-1}$ (arbitrary unit), respectively. As expected, the variants that did not express V-PPase, Y299A, A306S, L307A, L317A and N318A, displayed low basal levels of activity. In addition, the proton pumping reactions of these variants were less than 10% of wild type (Fig. 2C), thus making it difficult to determine their coupling efficiencies (Fig. 2D, those with asterisks). Moreover, mutation of amino acids in the front-end of TM6, such as that at L295 and F296, also decreased PP_i hydrolysis activity (<20% of wild type), indicating that the amino acids are essential for enzymatic activity (Fig. 2B). Several other mutant V-PPases, S298A, E301A, S313A, and F315A, retained about 30–50% PP_i hydrolysis of wild type; however, the rest of the mutants possessed relatively similar

enzymatic activities (>80%) as the control. The proton transport of the L295A, F296A, S298A, E301A, A305S, A310S, S313A, G316A and H319A mutants was only 10–40% of the wild type. These mutants exhibited a gross impairment in both PP_i-hydrolyzing and proton-translocating abilities, suggesting their crucial roles in maintaining the structure and function of V-PPase. However, the E301A mutation decreased coupling efficiency to 25% of the wild type (Fig. 2C and D), indicating its direct involvement in proton translocation by V-PPase.

3.2. Subcellular localization of V-PPase in mutants

To explain the absence of V-PPase expression on microsomal membranes in some variants, indirect immunofluorescence was used to examine protein distribution. The negative control (wild-type yeast cell stain with secondary antibody alone) was used to verify the absence of non-specific binding of antibody probes to V-PPase. From the confocal image, the wild-type V-PPase was observed to localize solely on the vacuolar membrane (Fig. 3B). The cells transfected with empty vectors displayed weak fluorescence signals as background. The L295A mutant, which showed low activity, could still be recognized by Western blotting but only on the vacuolar membrane, a pattern similar to wild type. The Y299A, A306S and L317A variants showed little or no V-PPase expression. The L307A and N318A mutants were more weakly expressed than wild type; additionally, their mutations abolished the targeting of the V-PPase and displayed broad cytosolic localization. The distribution of these mutant V-PPases in cell was further confirmed by Western blotting analysis on cytosolic and membrane fractions, respectively (Fig. 3C). The wild-type V-PPase was detected only in membrane fraction, while those of L307A and N318A mutants in the cytosolic fraction alone, concurring with the results from immunofluorescence analysis on yeast cells above (Fig. 3B). In addition, the V-PPases of Y299A, A306S and L317A mutants were absent either in cytoplasmic or in membrane fractions. Taken together, the amino acid residues along TM6 might play roles in protein expression and in the targeting of V-PPase to the appropriate microsomal membranes.

3.3. Proteolytic analysis of V-PPase

Microsomes containing V-PPase were treated with trypsin and then visualized by Western blotting (Fig. 4). Upon incubation with TPCK-treated trypsin at a protein/protease ratio of 50:1 (w/w) at 37 °C for 15 min, V-PPase was considerably digested. Addition of the physiological substrate Mg_2PP_i could partially prevent the digestion of V-PPase by trypsin [cf., 12]. Under similar conditions, several of the mutated V-PPase proteins, L295A, G297A, F315A, G316A and H319A, could be digested but were also protected by Mg_2PP_i in a way similar to wild type. However, the A300S, E301A, S302A, and S303A mutants were relatively resistant to proteolysis; the rest of the mutant proteins exhibited higher sensitivities. The mutation at these residues might induce a conformational change varying the degree of the vulnerability by trypsin attack. Additionally, the presence of the physiological substrate Mg_2PP_i caused partial protection for mutant H^+-PPases against trypsinolysis (Fig. 4). It is possible that the binding of physiological substrate might result in a conformational change of V-PPase, thus hindering the trypsin digestion [18,21,24].

Table 1
Kinetic parameters of mutant V-PPases. V_{max} and K_M values were obtained from Lineweaver–Burk plots using Sigmaplot 7.0 software (SPSS, Chicago, IL, USA). EA_{65}/EA_{37} denotes the ratio of enzymatic activities of variants at 37 °C to 65 °C, respectively.

Clone	V_{max}	K_M	pH optimum	Thermal stability
	[μmol PP_i (mg protein · h)$^{-1}$]	(μM)		EA_{65}/EA_{37} (%)
Vector	–	–	–	–
WT	54.9 ± 0.2	147.4 ± 7.4	7.7	55.9 ± 8.2
L295A	–	–	–	–
F296A	–	–	–	–
G297A	48.5 ± 0.2	155.5 ± 7.3	7.6	61.7 ± 1.9
S298A	9.3 ± 0.3	129.0 ± 8.2	7.5	49.8 ± 4.2
Y299A	–	–	n.d.	n.d.
A300S	33.1 ± 0.2	72.1 ± 6.3	7.7	42.3 ± 6.3
E301A	8.4 ± 0.1	14.7 ± 2.7	7.3	7.3 ± 3.7
S302A	41.7 ± 0.2	67.1 ± 6.0	7.9	45.4 ± 3.4
S303A	32.0 ± 0.2	72.0 ± 7.6	7.5	53.9 ± 4.9
C304A	41.5 ± 0.2	78.3 ± 6.4	7.5	41.9 ± 4.0
A305S	40.8 ± 0.2	79.1 ± 6.3	7.7	57.4 ± 7.1
A306S	–	–	n.d.	n.d.
L307A	–	–	n.d.	n.d.
V308A	55.3 ± 0.2	129.6 ± 5.6	7.8	48.5 ± 4.5
V309A	36.6 ± 1.4	61.2 ± 4.7	8.0	52.8 ± 4.5
A310S	34.0 ± 0.2	110.7 ± 7.3	7.8	47.8 ± 3.3
S311A	57.1 ± 0.2	97.8 ± 7.5	7.8	54.2 ± 2.8
I312A	36.9 ± 0.2	87.3 ± 4.9	7.7	44.0 ± 3.7
S313A	17.5 ± 0.1	35.0 ± 4.3	7.7	41.0 ± 2.3
S314A	39.4 ± 0.2	66.2 ± 6.7	7.8	46.8 ± 1.6
F315A	25.0 ± 0.2	62.6 ± 7.6	7.9	39.8 ± 4.3
G316A	28.1 ± 0.3	111.0 ± 9.4	7.8	26.0 ± 2.3
L317A	–	–	n.d.	n.d.
N318A	–	–	n.d.	n.d.
H319A	36.0 ± 0.2	79.5 ± 6.3	7.6	50.8 ± 2.1

3.4. The characteristics of TM6 mutants

A Lineweaver–Burk plot of wild-type V-PPase yielded apparent K_M and V_{max} values of 147.4 ± 7.4 μM and 54.9 ± 0.2 μmol PP_i consumed (mg protein · h)$^{-1}$, respectively. The apparent K_M and V_{max} values of each mutant were also determined and are summarized in Table 1. Because enzymatic activities of the L295A, F296A, Y299A, A306S, L307A, L317A and N318A mutants were almost abolished, kinetic parameters of these mutants were not determined. The apparent V_{max} and K_M values of the G297A, V308A and S311A mutants were similar to wild type. The apparent V_{max} value of S298A was slightly different from wild type, even though their apparent K_M values were similar.

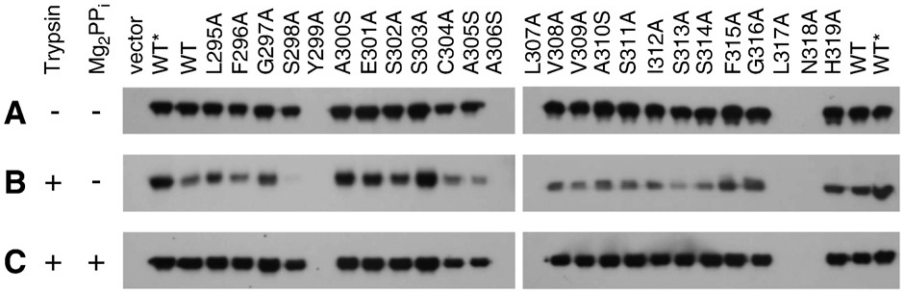

Fig. 4. The proteolytic analysis of V-PPase. (A) Control without trypsin treatment. (B) Treatment with trypsin. (C) Treatment with trypsin in the presence of Mg_2PP_i. Microsome membrane fractions (30 μg of protein each) were incubated with trypsin at a protein/ trypsin ratio of 50:1 (w/w) at 37 °C for 15 min followed by Western blotting analysis as described under Materials and methods. Protection was performed by incubating V-PPase with 2 mM Mg_2PP_i for 10 min on ice before trypsin treatment. The asterisk symbols (*) indicate the wild type protein without pre-treatment with trypsin.

However, both V_{max} and K_M values of the other mutants were decreased. Among these mutants, the apparent V_{max} and K_M values of E301A and S313A mutants were 10–30% of the wild type. The modifications in K_M values presumably suggest conformational changes due to mutations at these residues. Furthermore, the optimal pH of the variants for enzymatic activities was determined and summarized in Table 1. The wild type and most mutated V-PPase proteins showed similar optimum pH values at approximately pH 7.7. However, mutation at E301 made the optimal pH more acidic by nearly 0.5 units, while the V309A mutant made the optimal pH more basic (pH 8.0).

The analysis of thermal stability provides structural information on an enzyme of interest. Microsomes containing mutant V-PPase were exposed to different temperatures for 10 min and then cooled in an ice bath for another 5 min; the enzymatic activities were then measured immediately. The ratios of enzymatic activities of mutant V-PPases at 37 °C to 65 °C (for EA_{65}/EA_{37}), were compared to show thermal stabilities [25]. The EA_{65}/EA_{37} ratio for wild type V-PPase was $55.9 \pm 8.2\%$. The EA_{65}/EA_{37} ratios of most mutant V-PPases were similar to the wild type. The EA_{65}/EA_{37} ratios of the mutants A300S, E301A, S302A, C304A, A310S, I312A, S313A, S314A, F315A and G316A were below 45% of the wild type. For E301A and G316A mutants, the EA_{65}/EA_{37} ratios were decreased to $7.3 \pm 3.7\%$ and $26.0 \pm 2.3\%$ of wild type, respectively.

Fig. 5 depicts the ion effects on the wild type and the mutant V-PPases. As previously indicated, because the enzymatic activities of Y299A, A306S, L307A, L317A and N318A variants were almost abolished, the ion effects of these variants were not observed (data not shown). Nevertheless, K^+ (50 mM) could stimulate PP_i hydrolysis of wild-type V-PPase by approximately 8-fold (Fig. 5A). The K^+ stimulation of enzymatic activity of the L295A, F296A, S298A, E301A, C304A, A305A, V308A, S313A and S314A variants were significantly decreased to half of wild type. In contrast, the G316A mutant showed a 10-fold increase in the sensitivity to K^+. The K^+-sensitivities of the other mutants were similar to wild type, retaining both higher enzymatic activities and K^+-stimulation. Furthermore, the PP_i hydrolytic activity of the wild-type V-PPase remained $23.6 \pm 1.32\%$ in the presence of 0.1 mM Ca^{2+} (Fig. 5B). The L295A, F296A, S298A, E301A, C304A, A305S, V308A, and S313A mutants seem less sensitive to Ca^{2+}, maintaining activity at 1.5-fold that of wild type in the absence of Ca^{2+}. However, the G316A mutant was more sensitive to Ca^{2+}, with inhibition significantly decreased to 0.6 fold of wild type. The degrees of Ca^{2+}-inhibition for the rest of variants along TM6 were similar to wild type. Na^+ is also known to inhibit the enzymatic activity of vacuolar H^+-PPase [3]. At 100 mM of Na^+, the enzymatic activity of vacuolar H^+-PPase was declined to about $42.7 \pm 3.6\%$ of control (Fig. 5C). The levels of Na^+-inhibition for G297A, E301A, A305S, V308A, V309A and F315A mutants were similar to wild type. Mutation at A300, S302, S303, A310, S311, I312, S313A, S314, G316 and H319 enhanced Na^+ inhibition to about 20% of remaining activities. However, the L295A, F296A, S298A, and C304A mutants partially released their Na^+-inhibitory efficacies. In addition, the PP_i

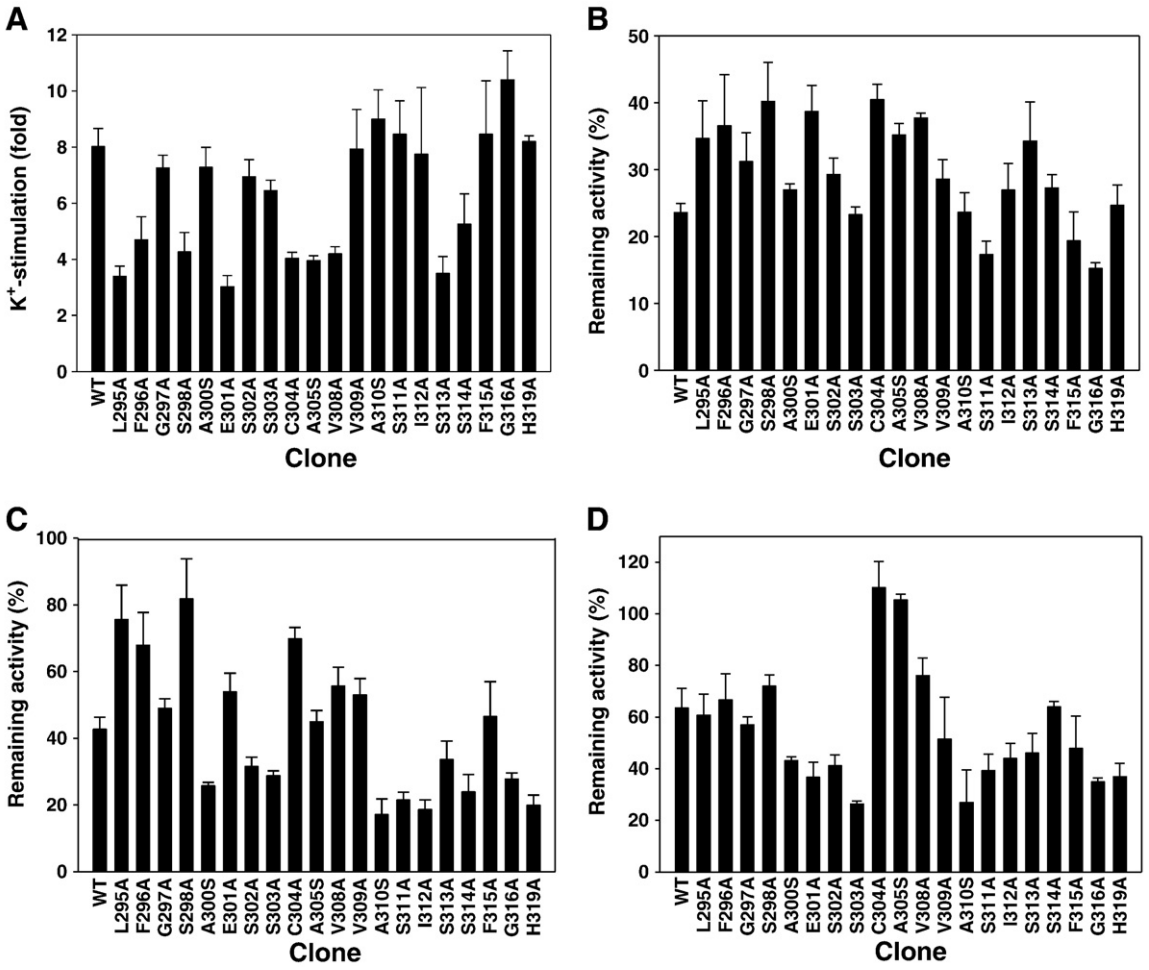

Fig. 5. Ion effects on V-PPase. (A) Potassium effects. (B) Calcium effects. (C) Sodium effects. (D) Fluoride effects. Microsomes containing heterologously expressed V-PPase were prepared from *S. cerevisiae* as described under Materials and methods. The concentrations of ions were: 50 mM K^+, 0.1 mM Ca^{2+}, 100 mM Na^+, and 10 mM F^-. Values are means ± standard deviation from at least three separate experiments.

hydrolytic activity of the wild type was decreased to 63.6 ± 7.5% in the presence of 10 mM F^- (Fig. 5D). The F^- inhibition of C304A and A305S mutants was abolished, whereas the enzymatic activities of A300S, E301A, S302A, S303A, A310S, S311A, I312A, S313A, G316A and H319A variants were further suppressed by F^-. In summary, of all mutants tested for ion effects, C304A lost sensitivity to all the ions examined. The L295A mutant also displayed similar sensitivity to these ions with the exception of F^-, and the A305S mutant showed similar responses to these ions with the exception of Na^+. Finally, the S311A and G316S mutants were more sensitive to K^+, Ca^{2+}, Na^+, and F^-.

4. Discussion

Analyses of cDNA and the determined amino acid sequences revealed that V-PPase contains 14–16 transmembrane domains with its catalytic side facing the cytoplasm [2,6]. These transmembrane segments may participate in proton translocation, structural stability and protein targeting. The alanine screening in this study showed that several amino acids along TM6 might be involved in these functions. The residues in the TM6 segment can be tentatively classified into three functional groups based on their roles in PP_i hydrolysis activity and coupling efficiency. The group I includes the amino acids (L295, F296, Y299, E301, A306, L307, S313, F315, L317 and N318) at which the mutation deteriorated both PP_i hydrolysis and coupling efficiencies. Among this group, such impairments in several mutants (Y299A, A306S, L307A, L317A and N318A) might come from the failure in protein expression. Notwithstanding, these amino acid residues primarily occupy one face of the helix wheel, called the "activity" face (Fig. 6A). Moreover, cellular localization assays revealed that Y299A, A306S, L307A, L317A and N318A mutants were not expressed efficiently or targeted properly onto microsomal membranes (Fig. 3B and C; discussed below). These residues were shown to be remarkably important for V-PPase conformational stability (Figs. 2 and 3). Furthermore, L295 and F296, residing at the beginning of transmembrane domain and near the catalytic site loop, were essential for catalytic function (Figs. 1A and 2). In addition, mutation at the highly conserved E301 residue also decreased enzymatic activity, in agreement with data showing that E305 of *A. thaliana*, which is equivalent to E301 of mung bean, is essential for catalysis through DCCD binding [11]. Besides, E301 locates on a face specifically relating to proton translocation (see below), indicating its possible role in proton pumping of V-PPase. Additionally, mutations at G297 and A305 residues, both of which are vertically adjacent to E301 along the helix wheel (Fig. 6B), decreased their coupling ratios, suggesting involvement in proton pumping, presumably through an appropriate conformation. Furthermore, the proteolysis assay showed that the A300S, E301A, S302A, and S303A mutants were relatively resistant to digestion, implying that mutation around this region along the helix wheel hinders trypsin attack, likely through consequential conformational changes.

The group II residues include G297, A305, V308, A310, G316, and H319, whose mutation decreased the coupling ratio but not PP_i hydrolysis activity, suggesting an impairment of proton translocation. Furthermore, these residues are located primarily at one face of the helix wheel, called the "proton-pumping" face (Fig. 6A). This face is opposite the activity face, implying they are either directly or indirectly involved in proton translocation (Fig. 6). It is conceivable that TM6 could be a part of the proton channel of V-PPase, as predicted from its relatively low hydrophobicity by hydropathic analysis [cf., 13]. Nevertheless, the exact structure and mechanism by which TM6 participates in proton translocation requires further investigation. Finally, the group III residues include S298, A300, S302, S303, C304, V309, S311, I312, and S314, whose mutation did not show significant changes in enzymatic reaction and coupling efficiency as compared to wild type, indicating that these residues are probably not essential for PP_i hydrolysis or H^+-translocation.

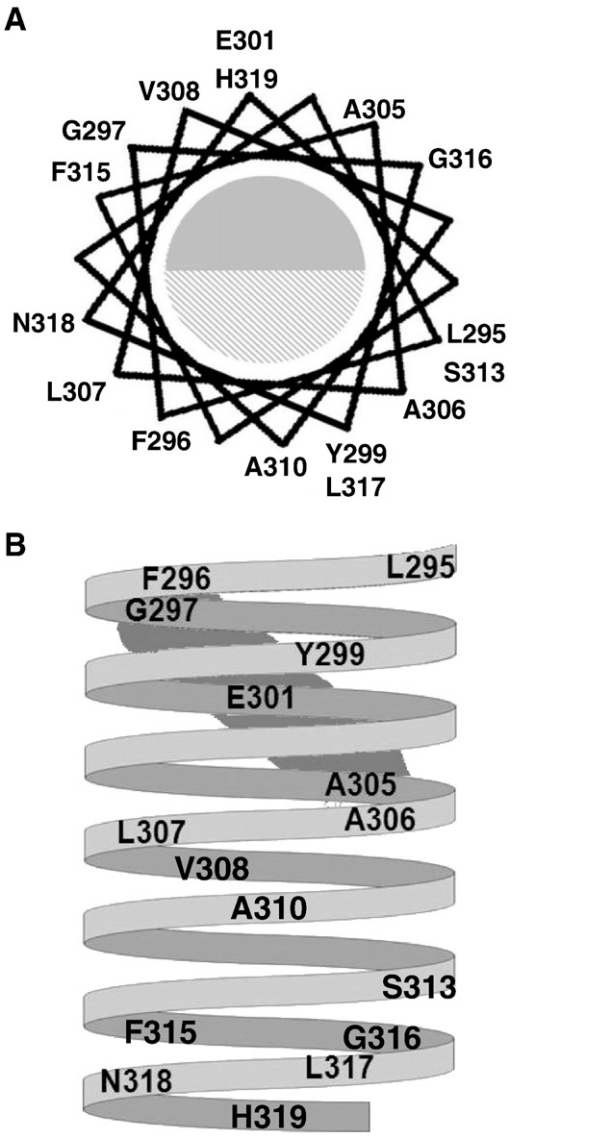

Fig. 6. Helix wheel of TM6. (A) Top view. (B) Side view. Only were the essential residues shown on the helix wheel presumably with one side (slashed) involved in PP_i hydrolysis (activity face) and the other (dark) involved in proton translocation (proton-pumping face).

Protein trafficking primarily involves signal peptides embedded within membrane proteins, and several distinct classes of sorting motifs have been well characterized [26,27]. For instance, it has been demonstrated that the motif residing within the fourth transmembrane domain determines the localization of the H,K-ATPase α subunit [28]. The apical sorting of two influenza virus proteins, neuraminidase and hemagglutinin, appears to be encoded in their transmembrane domains [29,30]. In this study, it was demonstrated that several mutant V-PPases were not expressed directly on microsomal membrane (Fig. 2A). Similar results were also found in other species, showing that specific single mutations might inhibit expression of V-PPase [cf., 6]. The current study demonstrated that the Y299A, A306S and L317A variants showed little or no V-PPase expression. In addition, the L307A and N318A mutants had markedly reduced cellular targeting, causing broad cytosolic localization. Helix wheel analysis shows that Y299, L306, and L317 were in one group and L307 and N318 were in another group located relatively close to each other on the same face of the wheel (cf., Fig. 6). It is speculated that TM6 of V-PPase may contain signal domains for its expression and targeting to the microsomal membrane.

V-PPase is sensitive to trypsinolysis, but the presence of Mg^{2+}-PP_i could protect it against the digestion [18,24], probably due to conformational change upon binding of the substrate complex. Mutations at several residues, A300, E301, S302, and S303, also provided relative protection against proteolysis, suggesting hindrance of the trypsin attack through conformational changes with mutation. However, the S298A and S313A mutants were more sensitive to the proteolysis as compared to wild type. The mutation at these residues most likely led to a more susceptible conformation for trypsin digestion. Furthermore, analysis of thermal sensibility in this study offers insights on the structural stability of V-PPase. Of all the variants, mutations at E301 and G316 dramatically increased the thermal sensitivity of V-PPase, indicating a role for these amino acids in maintaining the structure of V-PPase. TM6 may participate in the maintenance of the architecture of V-PPase, mediating the different vulnerabilities of the mutants to trypsin and heat attacks.

There are two main isoforms of V-PPase with different sensitivities to K^+-stimulation [2,31]. Evidence demonstrates that replacement of A460 of V-PPase from *Carboxydothermus hydrogenoformans* with lysine successfully turned the enzyme from the K^+-sensitive into the K^+-insensitive form, suggesting K^+ binding at this site [31]. In this study, it was further found that the C304A mutant possessed high enzymatic activity but was less sensitive to K^+ stimulation and Ca^{2+}, Na^+, and F^- inhibition. Sequence alignment indicates that the C304 of mung bean, which is equivalent to C308 of *A. thaliana*, is highly conserved. It is conceivable that the C304 residue resides in the vicinity of the domain directly or indirectly accommodates these ions. Furthermore, the L295 is more resistant to K^+, Ca^{2+}, and Na^+ effects, suggesting its similar role in ion binding.

In summary, this work shows that the Y299, A306, L307, L317 and N318 residues on one face of the helix wheel of TM6 (activity face) were essential for the enzymatic activities of V-PPase. On this face, the L307 and N318 residues are probably involved in the cellular localization of V-PPase. Moreover, some residues on the other face (the proton-pumping face) may play an essential role in the proton translocation by V-PPase. On this face, E301 is the most critical residue for proton transport. The roles of the amino acid residues along TM6 in the structural maintenance of V-PPase were elucidated by the investigation of proteolysis sensitivity, thermal stability, ion effects and expression of mutant proteins.

Acknowledgments

We thank Mr. Hui-Hao Lin for his technical assistance on confocal microscopy. This work was supported by grants from National Science Council, Taiwan to R.L. Pan (NSC 97-2311-B-007-003MY3 and NSC 97-2627-M-007-003) and CGMH-NTHU Joint Research No. 96N2421E1 to R.L. Pan.

References

[1] A. Serrano, J.R. Perez-Castineira, H. Baltscheffsky, M. Baltscheffsky, Proton-pumping inorganic pyrophosphatases in some archaea and other extremophilic prokaryotes, J. Bioenerg. Biomembr. 36 (2004) 127–133.
[2] Y.M. Drozdowicz, P.A. Rea, Vacuolar H^+-pyrophosphatases: from the evolutionary backwaters into the mainstream, Trends Plant Sci. 6 (2001) 206–211.
[3] M. Maeshima, Vacuolar H^+-pyrophosphatase, Biochim. Biophys. Acta 1465 (2000) 37–51.
[4] J.J. Wu, J.T. Ma, R.L. Pan, Functional size analysis of pyrophosphatase from *Rhodospirillum rubrum* determined by radiation inactivation, FEBS Lett. 283 (1991) 57–60.
[5] S.J. Yang, S.S. Jiang, R.C. Van, Y.Y. Hsiao, R.L. Pan, A lysine residue involved in the inhibition of vacuolar H^+-pyrophosphatase by fluorescein 5'-isothiocyanate, Biochim. Biophys. Acta 1460 (2000) 375–383.
[6] M. Hirono, Y. Nakanishi, M. Maeshima, Identification of amino acid residues participating in the energy coupling and proton transport of *Streptomyces coelicolor* A3(2) H^+-pyrophosphatase, Biochim. Biophys. Acta 1767 (2007) 1401–1411.
[7] H. Mimura, Y. Nakanishi, M. Hirono, M. Maeshima, Membrane topology of the H^+-pyrophosphatase of *Streptomyces coelicolor* determined by cysteine-scanning mutagenesis, J. Biol. Chem. 279 (2004) 35106–35112.
[8] Y.M. Drozdowicz, J.C. Kissinger, P.A. Rea, AVP2, a sequence-divergent, K^+-insensitive H^+-translocating inorganic pyrophosphatase from *Arabidopsis*, Plant Physiol. 123 (2000) 353–362.
[9] G.A. Belogurov, M.V. Turkina, A. Penttinen, S. Huopalahti, A.A. Baykov, R. Lahti, H^+-pyrophosphatase of *Rhodospirillum rubrum*. High yield expression in *Escherichia coli* and identification of the Cys residues responsible for inactivation by mersalyl, J. Biol. Chem. 277 (2002) 22209–22214.
[10] Y.M. Drozdowicz, Y.P. Lu, V. Patel, S. Fitz-Gibbon, J.H. Miller, P.A. Rea, A thermostable vacuolar-type membrane pyrophosphatase from the archaeon *Pyrobaculum aerophilum*: implication for the origins of pyrophosphate-energized pumps, FEBS Lett. 460 (1999) 505–512.
[11] R.G. Zhen, E.J. Kim, P.A. Rea, Acidic residues necessary for pyrophosphate-energized pumping and inhibition of the vacuolar H+-pyrophosphatase by N, N'-dicyclohexylcarbodiimide, J. Biol. Chem. 272 (1997) 22340–22348.
[12] Y. Nakanishi, T. Saijo, Y. Wada, M. Maeshima, Mutagenic analysis of functional residues in putative substrate-binding site and acidic domains of vacuolar H^+-pyrophosphatase, J. Biol. Chem. 276 (2001) 7654–7660.
[13] M.G. Claros, G.V. Heijne, TopPred II: an improved software for membrane protein structure predictions, CABIOS 10 (1994) 685–686.
[14] R.C. Van, Y.J. Pan, S.H. Hsu, Y.T. Huang, Y.Y. Hsiao, R.L. Pan, Role of transmembrane segment 5 of the plant vacuolar H^+-pyrophosphatase, Biochim. Biophys. Acta 1709 (2005) 84–94.
[15] S.H. Hung, S.J. Chiu, L.Y. Lin, R.L. Pan, Vacuolar H^+-pyrophosphatase cDNA (Accession No. U31467) (PGR 95-082) from etiolated mung bean seedlings, Plant Physiol. 109 (1995) 1–125.
[16] S. Barik, in: B.A. White (Ed.), PCR Cloning Protocols: From Molecular Cloning to Genetic Engineering, Humana Press Inc, New Jersey, USA, 1997, pp. 173–182.
[17] E.J. Kim, R.G. Zhen, P.A. Rea, Site-directed mutagenesis of vacuolar H^+-pyrophosphatase. Necessity of Cys634 for inhibition by maleimides but not catalysis, J. Biol. Chem. 270 (1995) 2630–2635.
[18] Y.Y. Hsiao, Y.J. Pan, S.H. Hsu, Y.T. Huang, T.H. Liu, C.H. Lee, C.H. Lee, P.F. Liu, W.C. Chang, Y.K. Wang, L.F. Chien, R.L. Pan, Functional roles of arginine residues in mung bean vacuolar H^+-pyrophosphatase, Biochim. Biophys. Acta 1767 (2007) 965–973.
[19] M. Bradford, A rapid and sensitive method for the quantitation of microgram quantities of protein utilizing the principle of protein dye binding, Anal. Biochem. 72 (1976) 248–254.
[20] U.K. Laemmli, Cleavage of structure proteins during the assembly of the head of bacteriophage T4, Nature (London) 222 (1970) 680–685.
[21] Y.Y. Hsiao, R.C. Van, S.H. Hung, H.H. Lin, R.L. Pan, Roles of histidine residues in plant vacuolar H^+-pyrophosphatase, Biochim. Biophys. Acta 1608 (2004) 190–199.
[22] M.C. Keogh, J.A. Kim, M. Downey, J. Fillingham, D. Chowdhury, J.C. Harrison, M. Onishi, N. Datta, S. Galicia, A. Emili, J. Lieberman, X. Shen, S. Buratowski, J.E. Haber, D. Durocher, J.F. Greenblatt, N.J. Krogan, A phosphatase complex that dephosphorylates H2AX regulates DNA damage checkpoint recovery in *S. cerevisiae*, Nature 439 (2006) 497–501.
[23] E.J. Kim, R.G. Zhen, P.A. Rea, Heterologous expression of plant vacuolar pyrophosphatase in yeast demonstrates sufficiency of the substrate-binding subunit for proton transport, Proc. Natl Acad. Sci. USA 91 (1994) 6128–6132.
[24] H.H. Lin, Y.J. Pan, S.H. Hsu, R.C. Van, Y.Y. Hsiao, J.H. Chen, R.L. Pan, Deletion mutation analysis on C-terminal domain of plant vacuolar H^+-pyrophosphatase, Arch. Biochem. Biophys. 442 (2005) 206–213.
[25] S.J. Yang, S.S. Jiang, Y.Y. Hsiao, R.C. Van, Y.J. Pan, R.L. Pan, Thermoinactivation analysis of vacuolar H^+-pyrophosphatase, Biochim. Biophys. Acta 1656 (2004) 88–95.
[26] J.S. Bonifacino, L.M. Traub, Signals for sorting of transmembrane proteins to endosomes and lysosomes, Annu. Rev. Biochem. 72 (2003) 395–447.
[27] T. Pawson, P. Nash, Assembly of cell regulatory systems through protein interaction domains, Science 300 (2003) 445–452.
[28] L.A. Dunbar, P. Aronson, M.J. Caplan, A transmembrane segment determines the steady-state localization of an ion-transporting adenosine triphosphatase, J. Cell Biol. 148 (2000) 769–778.
[29] A. Kudru, R.T. Avalos, C.M. Sanderson, D.P. Nayak, Transmembrane domain of influenza virus neuraminidase, a type II protein, possesses an apical sorting signal in polarized MDCK cells, J. Virol. 70 (1996) 6508–6515.
[30] S. Lin, H.Y. Naim, A.C. Rodriguez, M.G. Roth, Mutations in the middle of the transmembrane domain reverse the polarity of transport of the influenza virus hemagglutinin in MDCK epithelial cells, J. Cell Biol. 142 (1998) 51–57.
[31] G.A. Belogurov, R. Lahti, A lysine substitute for K^+ A460K mutation eliminates K^+ dependence in H^+-pyrophosphatase of *Carboxydothermus hydrogenoformans*, J. Biol. Chem. 277 (2002) 49651–49654.
[32] S. Subramaniam, The Biology Workbench—a seamless database and analysis environment for the biologist, Proteins 32 (1998) 1–2.